JOURNAL OF THE AMERICAN CHEMICAL SOCIETY

Article

pubs.acs.org/JACS

Selective Cleavage of Periodic Mesoscale Structures: Two-Dimensional Replication of Binary Colloidal Crystals into Dimpled Gold Nanoplates

Yoshiyuki Kuroda,[†,||] Yasuhiro Sakamoto,[‡] and Kazuyuki Kuroda*[,†,§]

[†]Department of Applied Chemistry, Faculty of Science and Engineering, Waseda University, 3-4-1 Ohkubo, Shinjuku-ku, Tokyo 169-8555, Japan

[‡]Nanoscience and Nanotechnology Research Center, Osaka Prefecture University, Sakai, Osaka 599-8570, Japan

[§]Kagami Memorial Research Institute for Materials Science and Technology, Waseda University, 2-8-26 Nishiwaseda, Shinjuku-ku, Tokyo 169-0051, Japan

Supporting Information

ABSTRACT: Specific crystallographic planes of binary colloidal crystals consisting of silica nanoparticles are two-dimensionally replicated on the surface of gold nanoplates. The selectivity of the surface patterns is explained by the geometrical characteristics of the binary colloidal crystals as templates. The binary colloidal crystals with the AlB_2- and $NaZn_{13}$-type structures are fabricated from aqueous dispersions of stoichiometrically mixed silica nanoparticles with different sizes. The stoichiometry is precisely controlled on the basis of a seed growth of silica nanoparticles. Dimpled gold nanoplates are formed by the two-dimensional growth of gold between partially cleaved surfaces of templates. The selectivity of the surface patterns is explained using the AlB_2-type binary colloidal crystal as a template. The surface pattern is determined by the preferential cleavage of the plane with the lowest density of particle−particle connections. The tendency to form well-defined cleavage in binary colloidal crystals is crucial to formation of dimpled gold nanoplates, which is explained using the $NaZn_{13}$-type binary colloidal crystal as a template. Its complex structure does not show well-defined cleavage, and only distorted nanoplates are obtained. Therefore, the mechanism of the two-dimensional replication of binary colloidal crystals is reasonably explained on the basis of their periodic mesoscale structures and crystal-like properties.

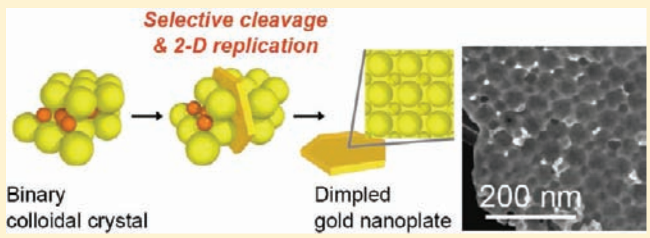

■ INTRODUCTION

Nanostructured metals with controlled morphologies have attracted much attention for their unique properties and potential applications in nanotechnology.[1] Nanostructures of metals are quite influential to their quantum-size effects, such as optical,[1,2] magnetic,[3] and catalytic properties.[4] Porous nanostructures are quite important for their applications as electrodes,[5] sensors,[6] and catalysts[7] because of their high surface area and efficient diffusion of guest molecules within pores. Morphological control of nanostructured metals into rods or sheets is also important for their anisotropic electronic and optical properties, applications for surface-enhanced Raman scattering (SERS),[8] and assemblies into hierarchical structures.

Gold is one of the most useful metals because of its exceptional chemical stability, conductivity, and unique optical[2] and catalytic properties.[7] Plasmonic materials, such as sensors, imaging materials, metamaterials, SERS substrates, etc., have intensively been explored using nanostructured gold.[2c] Not only gold nanoparticles but also nanoporous gold is promising as a catalyst.[7] Morphosynthesis of gold with various nanoscale shapes, such as polyhedrons,[9] rods,[10,11] and plates,[12,13] has been developed in recent years. Formation of unique shapes has been systematically examined, based on anisotropic crystal growth by the presence of organic molecules,[10] polymers,[9,12] or metal ions.[11] Crystalline defects, such as stacking faults, also lead to formation of complex shapes which are difficult to be formed only by anisotropic crystal growth.[9,11,13] Although porous nanostructures of metals have been prepared by replication of surfactants,[14−16] block copolymers,[17] and mesoporous silica,[14,18] formation of porous gold is quite difficult because of undesired overgrowth of gold within templates.[15]

We recently reported the formation of nanostructured gold with platelike morphology by a unique two-dimensional replication of a colloidal crystal consisting of silica nanoparticles whose arrangement is the face-centered cubic (fcc) structure.[19] Gold nanoplates with highly ordered dimples on their surfaces, which we call dimpled gold nanoplates, are formed by the method. Only two-dimensional parts of nanostructures of templates are replicated with gold by the two-dimensional crystal growth of gold between partially cleaved surfaces of

Received: March 17, 2012
Published: April 23, 2012

ACS Publications © 2012 American Chemical Society

dx.doi.org/10.1021/ja3026054 | J. Am. Chem. Soc. 2012, 134, 8684−8692

templates. The colloidal crystals act not only as rigid templates of dimpled nanostructures but also as flexible reaction spaces for morphosynthesis of nanoplates. Such a flexibility of templates is important to overcome the difficulty of the synthesis of nanostructured gold and extends the diversity of nanostructures and morphologies of replicas. Because the dimpled gold nanoplates are mostly single crystalline, formation of dimples is expected to be effective to create high-index surfaces with many steps or kinks on the surface of gold, which is crucial to highly active catalysts.[20]

The most interesting point of our previous report is the selectivity of the growth direction of gold nanoplates within the three-dimensional interstitial nanospace of colloidal crystals. The dimples on the surface of gold nanoplates were mostly arranged with hexagonal symmetry, which implies that gold grows selectively in the {111} plane of the fcc structure. The reason for the selectivity was explained by the preferential cleavage of colloidal crystals on the {111} planes because their surface energy is lowest among those in the fcc structure.[21] Cleavage due to growth of gold nanoplates within their interstitial nanospace probably distinguishes small differences in the strength and geometries of local bonds among nanoparticles. No characteristic relationships were observed between the crystal orientation of gold and the platelike morphology, which suggests that the platelike morphology is controlled by the limitation of the growth of gold in the two-dimensional nanospaces between the cleaved surfaces. The mechanism of the morphosynthesis is totally different from the previous ones of anisotropic crystal growth of gold along specific crystalline directions.[9−13] This is surprising because growing gold selects specific nanospaces in colloidal crystals, which has opened a new door for the utilization of *periodic* mesoscale structures with three-dimensional architectures. Xia et al. also reported the use of nanoparticle arrays as flexible templates, whereas such a selective growth was not observed.[22] Similar ZnO nanoplates with highly ordered dimples were also formed by their preferential growth in the fcc-{111} planes of a colloidal crystal consisting of polystyrene particles,[23] though the size of the template was on the submicrometer scale (polystyrene particles ca. 270 nm in size). It was discussed that the growth direction of ZnO nanoplates was affected by the larger interplanar distance of the {111} plane than the {110} and {100} planes. Holes penetrating through the nanoplates indicated that the cleavage of colloidal crystals did not occur. Therefore, the size of nanospaces is suggested to be important for cleavage of colloidal crystals. Two-dimensional replication is expected to have great potential to create a new field of the syntheses of metal nanostructures. A deeper understanding of the mechanisms underlying the nucleation and growth of metal nanostructures within and beyond the colloidal lattice is expected to design and synthesize nanostructures more complex than anything currently available.[24] However, the understanding of mechanisms of the two-dimensional replication is quite limited because we used the colloidal crystal possessing only the fcc structure. It is essential to develop a new colloidal crystal system to extend the variety of mesoscale structures.

Binary systems of stoichiometrically mixed nanoparticles with two different sizes[25,26] are quite promising to vary nanostructures of colloidal crystals. Diverse crystallographic arrangements of nanoparticles in binary nanoparticle superlattices (BNSLs) have been achieved.[25] Even though enhanced physical properties (e.g., conductance and magnetoresistance) of BNSLs have been shown,[26] the relationships between their functions and their periodic mesoscale structures are still unclear. Various nanostructures are expected to form by the synergistic combination of two-dimensional replication and various binary superlattices because nanostructural and morphological features of products are highly dependent on the three-dimensional periodic arrangements of nanoparticles. However, organically capped nanoparticles cannot be used as templates of gold because continuous networks of inorganic materials are not present.

Binary colloidal crystals consisting of silica nanoparticles with different particle sizes are promising for this purpose because silica nanoparticles are covalently connected on their surfaces. However, such binary colloidal crystals have not been prepared in mesoscale,[27] though those consisting of submicrometer-scale colloidal silicas occur as natural opals[28] and limited examples using colloidal silicas and polymers in submicrometer scale were reported.[29] Therefore, we focused on the use of monodispersed silica nanoparticles with much smaller sizes reported by Yokoi et al. and Tsapatsis et al.[30] Periodic arrangements of the nanoparticles in unary system have been achieved by simple solvent evaporation. The solvent evaporation process allows us to form a relatively large amount of colloidal crystals. Because the surface of silica nanoparticles is not covalently capped with organic molecules, it is also important to understand the assembling behavior of silica nanoparticles with different particle sizes. On the other hand, it is generally complicated to control the stoichiometry of small and large nanoparticles during formation of binary colloidal crystals because the number of nanoparticles is difficult to be estimated. We also focused on the seed-growth process of silica nanoparticles.[31] The number of nanoparticles is in principle not changed during the growth process, which is ideal to the stoichiometrically controlled fabrication of binary colloidal crystals. This concept can be extended to the control of BNSLs.

Herein, we report the preparation of binary colloidal crystals consisting of silica nanoparticles with different particle sizes and their application to two-dimensional replication for formation of dimpled gold nanoplates possessing various surface patterns (Scheme 1). We found that specific crystallographic planes of binary colloidal crystals can be used as a a two-dimesnional template, and its selectivity can be explained by the preference of the planes to be cleaved, determined by the density of particle−particle connections on each plane.

■ EXPERIMENTAL SECTION

Materials. L-Lysine (Sigma-Aldrich Co.) and tetraethoxysilane (TEOS, Kishida Chemical Co.) were used for synthesis of silica nanoparticles. $HAuCl_4 \cdot 4H_2O$ (Kanto Chemical Co., Inc.) was used as a metal source. Dimethylamineborane (DMAB, Wako Pure Chemical Ind. Ltd.) was used as a reducing agent. Hydrofluoric acid (Wako Pure Chemical Ind. Ltd.) and ethanol (Kanto Chemical Co., Inc.) were used for removal of templates. All chemicals were used without further purification.

Synthesis of Silica Nanoparticles with Different Particle Size. Silica nanoparticles were synthesized by the modified Stöber method according to the literature by Yokoi et al.[30] An aqueous dispersion containing silica nanoparticles 12 nm in size was prepared by stirring a reaction mixture containing L-lysine (0.097 g), TEOS (7.4 mL), and deionized water (100 mL) at 60 °C for 20 h. The particle size was increased on the basis of the seed-growth method, in which an appropriate amount of nanoparticle dispersion was added into an unreacted reaction mixture and stirred at 60 °C for 20 h. The ratio of the nanoparticle dispersion and the unreacted mixture was determined by the following formula[31]

Scheme 1. Schematic Illustration of the Two-Dimensional Replication To Form Dimpled Gold Nanoplates with Various Surface Patterns Using (a) Binary Colloidal Crystals and (b) a Unary Colloidal Crystal

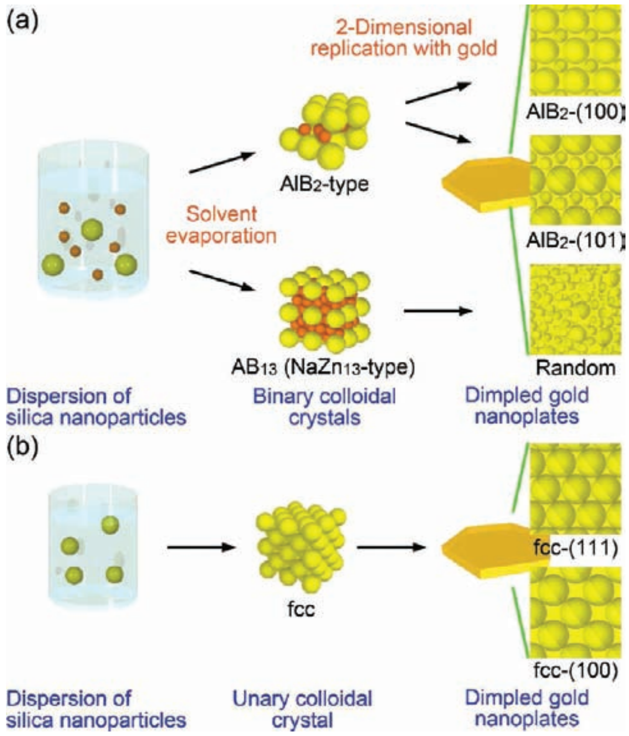

Scheme 2. (a) Formation of Nanoparticle Dispersions Containing the Same Numbers of Small and Large Silica Nanoparticles. (b) Formation of a Binary Colloidal Crystal (AB_2) from the Nanoparticle Dispersions

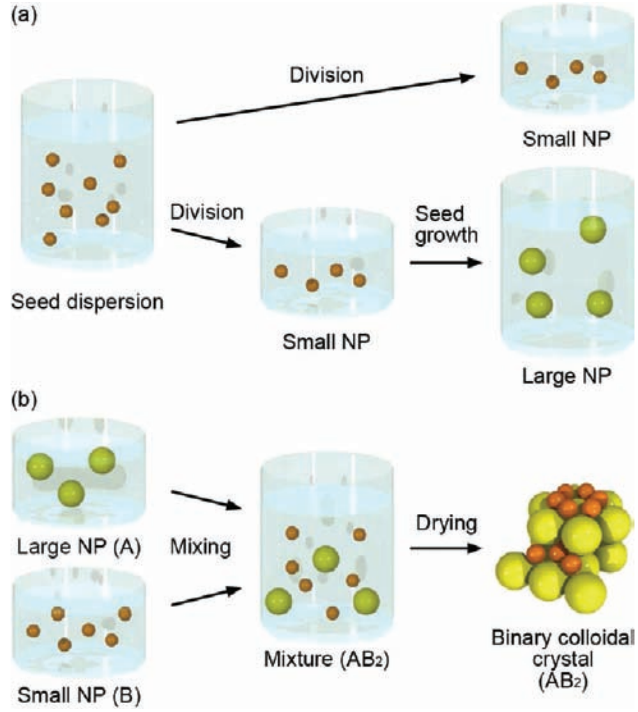

$$\left(\frac{\text{Diameter}_{\text{final}}}{\text{Diameter}_{\text{seed}}}\right)^3 - 1 = \frac{\text{Mass}_{\text{TEOS,added}}}{\text{Mass}_{\text{TEOS,seed}}}$$

The particle size is monodispersed (standard deviation is 4−6%), which is sufficient to form periodic colloidal crystals.

To control the stoichiometry of small and large nanoparticles for fabrication of binary colloidal crystals, a nanoparticle dispersion was divided into two parts (Scheme 2a). One was used as the dispersion of small nanoparticles. The other was used as the seed dispersion of large nanoparticles. Because all TEOS molecules are used for growth of seed nanoparticles, the number of nanoparticles in the seed dispersion is retained during the growth process.[31,32] The stoichiometry of small and large nanoparticles was controlled by the volume of dispersions.

Formation of Binary Colloidal Crystals. The stoichiometrically controlled dispersions containing small and large nanoparticles were mixed according to Table 1 (Scheme 2b). The larger and smaller ones are denoted as **A** and **B** nanoparticles, respectively. The ratio of the particle sizes is denoted as α. The solvent in the mixture was evaporated at 80 °C or room temperature. The flakes obtained after solvent evaporation were heat treated at 550 °C for 3 h in air to remove organic moieties.

Formation of Dimpled Gold Nanoplates. Dimpled gold nanoplates were prepared by the method reported previously.[19] A flaky binary colloidal crystal (0.2 g) was ground in a mortar and dried under vacuum overnight. An aqueous solution (40 μL) containing 0.2 M $HAuCl_4$ was mixed with the powdery binary colloidal crystal. After the composite was dried under vacuum, a $HAuCl_4$ solution (40 μL) was additionally mixed with the composite and dried under vacuum. The composite and DMAB were placed in a closed vessel overnight, which allowed reduction of $HAuCl_4$ to Au(0) in the interstices of silica nanoparticles. The reduced composite was mixed with 5% HF solution (10 mL) to dissolve silica nanoparticles completely. The present conditions are the same as those in our previous report using unary colloidal crystals as templates,[19] in which complete reduction of $HAuCl_4$ to metallic gold and removal of silica templates have been confirmed by the X-ray diffraction technique and energy-dispersive X-ray analyses.

Characterization. High-resolution scanning electron microscopy (HRSEM) images and bright-field scanning transmission electron microscopy (BFSTEM) images were taken using a Hitachi S-5500 microscope. Transmission electron microscopy (TEM) images were taken using a JEOL JEM-2010 microscope. Samples were crushed with ethanol on a mortar and mounted on Cu grids coated by a holey carbon film without any metal coating for both SEM and TEM observation. HRSEM images were treated with noise reduction using Adobe Photoshop CS5. The fast Fourier transform (FFT) was performed by DigitalMicrograph (Gatan, Inc.).

■ RESULTS AND DISCUSSION

Structures of Binary Colloidal Crystals. All binary colloidal crystal samples are flaky solids whose size is a few millimeters. Transparent flakes could be prepared by slow evaporation of solvent (see Supporting Information). Even though they were prepared by simple solvent evaporation, ordered binary colloidal crystals were obtained. Yokoi et al. discussed that the buffering action of L-lysine during solvent evaporation is crucial to formation of ordered unary colloidal crystals without aggregation,[30d] which is probably applied in the same way for the present case. Arrangements of nanoparticles with a higher packing density than that of the fcc structure are predicted on the basis of the hard-sphere approximation.[33] The arrangements can be varied by the stoichiometry of nanoparticles and the α value. Because the stoichiometries of nanoparticles were exactly controlled, multiple phases of ordered binary colloidal crystals were rarely observed for the AB_2 stoichiometry. In the case of AB_{13} stoichiometry, a small amount of unary colloidal crystals consisting of **B** nanoparticles was also segregated.

Table 1. Structural Parameters of Binary Colloidal Crystals Consisting of Silica Nanoparticles

			A nanoparticles		B nanoparticles		.
sample	stoichiometry	α^a	average size/nm	std. %	average size/nm	std. %	structural analogue
$AB_2(0.50)$	AB_2	0.50	51	4	26	5	AlB_2
$AB_{13}(0.54)$	AB_{13}	0.54	35	6	19	6	$NaZn_{13}$

[a]Ratio of the average particle size of **B** (smaller one) over the particle size of **A** (larger one).

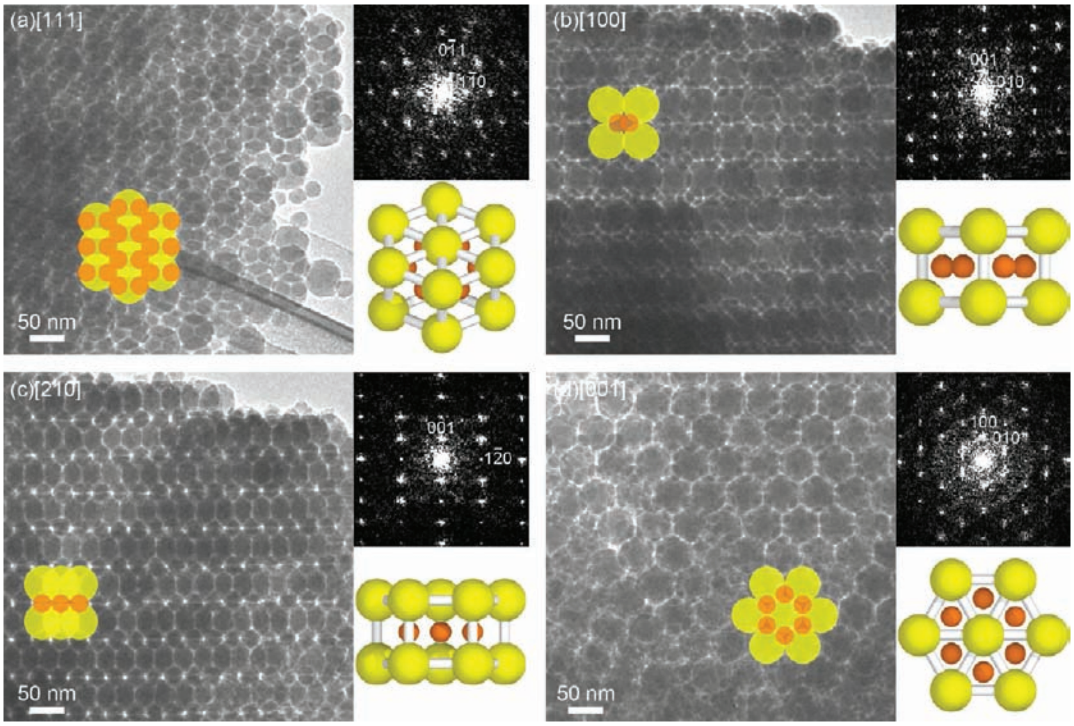

Figure 1. TEM images of $AB_2(0.50)$ with the AlB_2-type structure viewed along the (a) [111], (b) [110], (c) [210], and (d) [001] directions. Yellow and orange filled circles indicate the positions of **A** and **B** nanoparticles, respectively. Right of the TEM images are (top) the corresponding FFT pattern and (bottom) the corresponding structural model. Models are displayed by sticks and balls to clarify their internal structures.

The structure of $AB_2(0.50)$ was assigned to the AlB_2 type ($P6/mmm$, SG191) from the TEM images along the [111], [110], [210], and [001] directions (Figure 1). The lattice constants a and c were estimated to be ca. 51 and 52 nm, respectively.[34] Some distortions were observed for the binary colloidal crystals, which is probably due to strains caused during the solvent evaporation process. Because nanoparticles are almost in close contact, the interstices of the silica nanoparticles are expected to be used as a reaction space for the two-dimensional replication into dimpled gold nanoplates.[19] The α value of 0.50 is close to the geometrically ideal value (α = 0.527) to achieve maximum contacts of both **A**–**A** and **A**–**B** connections.

When α is 0.54 for the AB_{13} stoichiometry, it is expected that $NaZn_{13}$-type ($Fm\overline{3}c$, SG226) structure is formed as a binary colloidal crystal of silica nanoparticles. This structure is observed in natural opals[28] and BNSLs.[34] In the $NaZn_{13}$-type structure, 13 **B** nanoparticles form an icosahedral cluster surrounded by 8 **A** nanoparticles to form a periodic structure with cubic symmetry. The TEM image of the product shows a periodic square-like arrangement of **A** nanoparticles, corresponding to the [100] projection of the $NaZn_{13}$-type structure (Figure 2a). The filtered image by FFT also indicates the ordering of **A** and **B** nanoparticles (Figure 2b and 2c). The AlB_2- and $NaZn_{13}$-type structures are consistent with those predicted by the hard-sphere approximation of packing of colloidal particles.[28] The present method by controlling the stoichiometries and particle sizes is ideal to explore the phase diagram of the binary colloidal system.

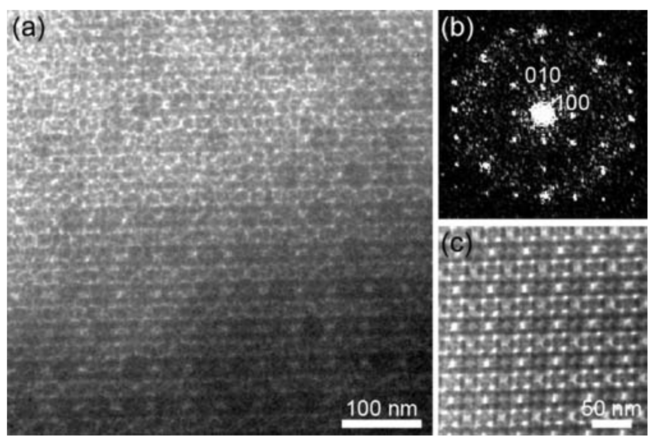

Figure 2. (a) TEM image of $AB_{13}(0.54)$, (b) its corresponding FFT pattern, and filtered image of a.

The tendency of cleavage is an important factor for the two-dimensional replication of binary colloidal crystals into dimpled gold nanoplates. HRSEM observation of the binary colloidal crystals shows their fractured surfaces formed by the crushing

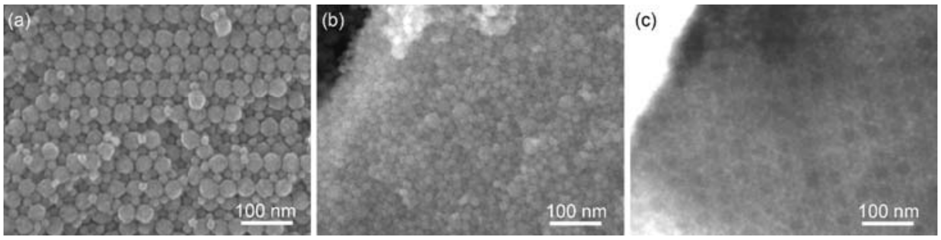

Figure 3. HRSEM images of fractured surfaces of (a) $AB_2(0.50)$ and (b) $AB_{13}(0.54)$. (c) BFSTEM image of $AB_{13}(0.54)$ at the same area as b.

process. A binary colloidal crystal with AlB_2-type structure shows well-defined cleaved surfaces on the fractured surface (Figure 3a). On the contrary, that with the $NaZn_{13}$-type structure shows rough surfaces even though the BFSTEM image of the same area shows a periodic structure inside the assembly (Figure 3b and 3c). Although the $NaZn_{13}$-type structure is highly ordered, the complex cluster-like arrangement of **B** nanoparticles in relatively small length scale probably changes the direction of cleavage propagation.

Surface Patterns of Dimpled Gold Nanoplates. The binary colloidal crystals presented here have unique structural features that are expected to be influential to two-dimensional replication. The difference is as follows. The AlB_2-type structure is useful to discuss the effects of three-dimensional arrangement of nanoparticles. It has two-dimensional arrangements of **A** nanoparticles with hexagonal and rectangular (almost square because a/c is ca. 1) symmetries on the {001} and {100} surfaces, respectively. These arrangements are similar to those of the {111} and {100} surfaces of the fcc structure, respectively, though the three-dimensional particle−particle connections are different from each other. The $NaZn_{13}$-type structure does not show well-defined cleavage, even though it has the well-defined periodicity. The tendency of formation of well-defined cleavage is thought to be influential to the platelike morphology of dimpled gold nanoplates.

Dimpled gold nanoplates were formed using $AB_2(0.50)$ with the AlB_2-type structure as a template (Figure 4a). Formation of dimpled gold nanoplates is due to partial cleavage of the template along the specific direction and two-dimensional growth of gold between the cleaved surfaces, which is suggested on the basis of their platelike morphology and the absence of holes penetrating through the nanoplate.[19] Ill-shaped particles formed by deposition of gold outside of binary colloidal crystals were also observed. They are formed possibly by diffusion of $[AuCl_4]^-$ ions outside of the templates. Their amount could be reduced by modifying the surface of silica nanoparticles with organic groups to control diffusion of $[AuCl_4]^-$ ions.

Two types of surface patterns were observed for the dimpled gold nanoplates formed in the AlB_2-type structure, and one of them was almost selectively observed. The major one is a lattice-like pattern of large and small dimples (Figure 4b), which corresponds to the structure of the {100} plane to be cleaved in the AlB_2-type structure. The minor one is a stripe-like arrangement of large and small dimples (Figure 4c), which corresponds to the {101} plane to be cleaved in the AlB_2-type structure. These results indicate that the two-dimensional arrangements of dimples are significantly different from those of the dimpled gold nanoplates formed in the fcc structure.[19]

When $AB_{13}(0.54)$ was used as the template, gold nanoplates with randomly arranged dimples were obtained (Figure 5). The product was not as flat as other dimpled gold nanoplates prepared using colloidal crystals with the fcc or AlB_2-type structures, which is consistent with the distorted geometry of the fractured surface of the template (Figure 3b).

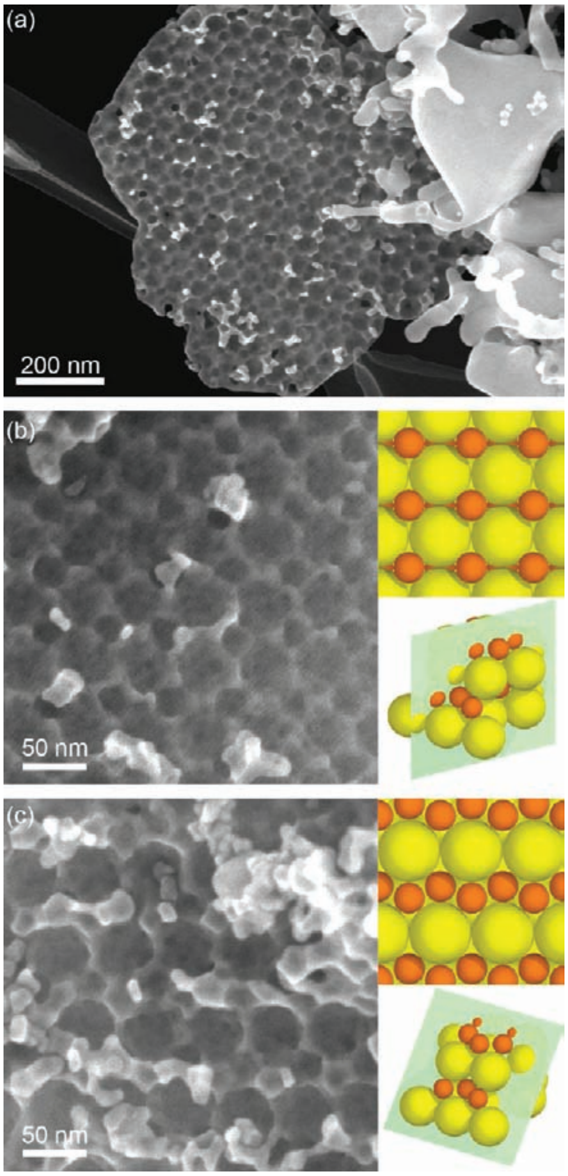

Figure 4. HRSEM images of dimpled gold nanoplates. (a) Low-magnification image. High-magnification images with (b) $AlB_2(100)$- and (c) $AlB_2(101)$-type surface patterns. Insets are (upper) the corresponding structural model and (lower) the indication of the cleaved surface in a three-dimensional model.

The selectivity of surface patterns of dimpled gold nanoplates can be explained by the preference of planes to be cleaved in templates because dimpled gold nanoplates were revealed to be formed between partially cleaved surfaces of colloidal crystals.[19]

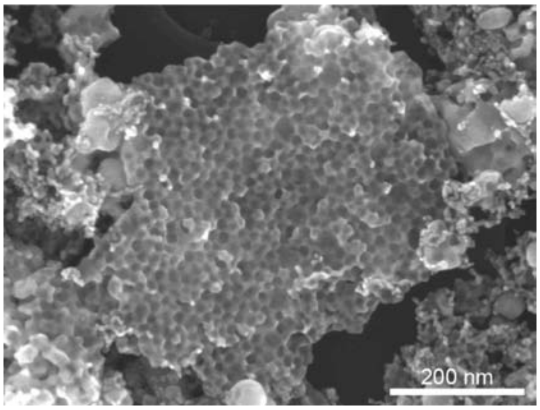

Figure 5. HRSEM image of the dimpled gold nanoplate replicated from $AB_{13}(0.54)$.

Once the colloidal crystal is partially cleaved, gold should grow rapidly between the cleaved surfaces with a larger nanospace than original interstitial nanospaces because of the efficient diffusion of $[AuCl_4]^-$. The initial growth direction of gold within a template before the occurrence of partial cleavage should be limited by the geometry of the three-dimensional interstitial nanospaces; however, such a limitation is immediately weakened due to the cleavages.

The preference of planes to be cleaved is probably determined by their bond strength. We here propose the density of particle–particle connections among silica nanoparticles on each plane as a decisive parameter to characterize the preference of planes to be cleaved. We hypothesize that the strains in colloidal crystals due to overgrowth of gold is basically isotropic to all directions because the crystal structure of gold is cubic. Therefore, the number of particle–particle connections per unit area of each plane is thought to be the parameter to discuss the preference of planes to be cleaved.

The densities of particle–particle connections on the planes to be cleaved in the AlB_2-type structure are summarized in Table 2. The densities are geometrically calculated from the models of the ideal AlB_2-type structure with $\alpha = 0.527$ (Figure 6). The diameter of an **A** nanoparticle is denoted as D. The connections to be disconnected upon cleavage were counted. Among these planes, the {100} plane has the lowest density of particle–particle connections (weak connection), which is consistent with the frequent observation of {100}-type surface patterns on dimpled gold nanoplates. {101} has the second lowest density, which is also consistent with the minor observation of the corresponding surface pattern. On the contrary, dimples arranged with hexagonal symmetry, corresponding to the {001} surface, were not observed as the surface pattern of dimpled gold nanoplates, even though such dimples arranged with hexagonal symmetry were quite frequently observed for dimpled gold nanoplates formed in the fcc structure.[19] This plane has a higher density of particle–particle connections than those of {100} and {101} planes. Therefore, the order of the density of particle–particle connections is well consistent with the frequency of the corresponding surface patterns on dimpled gold nanoplates.

Table 2. Density of Connections of Each Plane To Be Cleaved in the AlB_2-Type Structure With an α Value of 0.527

plane	cross-sectional area of the unit cell $(A)^a$	number of **A**–**A** connections in two-dimensional unit cell (N_A)	number of **A**–**B** connections in two-dimensional unit cell (N_B)	density of connections ($(N_A+N_B)A^{-1}$)
{100}	1	2	4	6
{101}	$\sqrt{7}/2$	3	6	6.8
{001}	$\sqrt{3}/2$	1	6	8.1

^{a}Cross-sectional area of the two-dimensional unit cell is normalized by D^2, where D is the diameter of the larger nanoparticle.

There are some deviations in $AB_2(0.50)$ from the ideal closely packed structure. The most significant deviation from the ideal structure is the α value. The α value was 0.50 in the present experiment, in which **B** nanoparticles are relatively smaller than those in the ideal closely packed structure. Therefore, the decrease in the α value for the AlB_2-type structure causes a decrease in the number of **A**–**B** connections, whereas **A**–**A** connections should be constant. When the number of **A**–**B** connections is more than 46.5% of the ideal number, the order of the densities of particle–particle connections does not change (see Supporting Information). Moreover, it is expected that particle–particle connections are also formed by shrinkage of colloidal crystals during heat treatment. Therefore, it is thought that the selectivity of surface patterns is not affected by such a small deviation of the α value.

The areas of contacts between silica nanoparticles should be influential to the bond strength of the planes to be cleaved. The area of contact in **A**–**A** connection is thought to be slightly larger than that in **A**–**B** connection because of the difference in sizes and surface curvatures of nanoparticles. However, it is quite difficult to estimate the difference in the areas of contacts because the size distributions of nanoparticles, the shapes of nanoparticles, and the surface conditions are influential to the areas of contacts.

The tendency was also observed for a unary colloidal crystal with the fcc structure. The densities of particle–particle connections on {111}, {100}, and {110} planes to be cleaved in the fcc structure are summarized in Table 3, which was calculated from the models in Figure 7. In our previous report using a unary colloidal crystal with the fcc structure[19] a hexagonal arrangement of dimples assignable to the {111} structure was observed for more than 90% of the dimpled gold nanoplates. Dimples arranged with square symmetry assignable to the {100} structure were observed to a much lesser extent. This order is consistent with the order of the calculated density of particle–particle connections.

The size of nanoparticles is also important for formation of dimpled gold nanoplates. When unary colloidal crystals consisting of silica nanoparticles ca. 15 nm in size, products have bulkier morphology (Figure S3, Supporting Information). Dimpled gold nanoplates were also formed using unary colloidal crystals ca. 60 nm in size as a template (Figure S4, Supporting Information). Other researchers have reported formation of three-dimensionally ordered macroporous gold using larger colloidal particles (typically more than 100 nm) as templates.[6b] Therefore, two-dimensional replication is a unique phenomenon on the mesoscale.

The present system gives a novel concept for creation of diverse mesoscale structures. The diversity of conventional mesoporous materials prepared using surfactant templates depends mainly on the packed structures of surfactant micelles. Various three-dimensional cage-type mesoscale structures were shown to be explained by soft-sphere packing of micelle templates, in which the interfacial area of the packed micelles is minimized.[35] On the other hand, the present system is based on

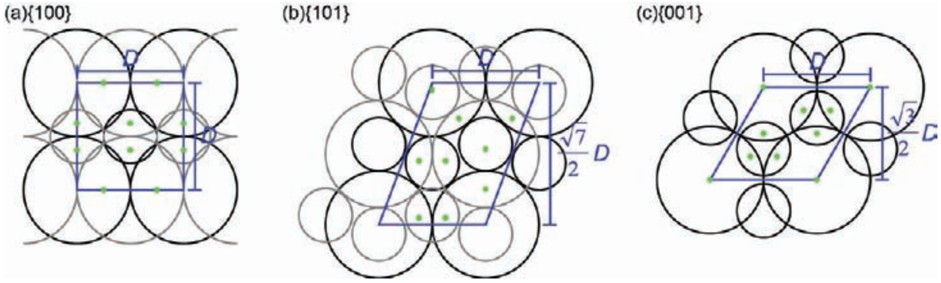

Figure 6. Models of the AlB_2-type structure on (a) {100}, (b) {101}, and (c) {001} planes. Black and gray lines indicate the outlines of nanoparticles on upper and lower layers of a cleavage, respectively. Blue lines indicate the two-dimensional unit cell of each plane. Green dots indicate particle–particle connections between the upper and the lower layers.

Table 3. Density of Connections of Each Plane To Be Cleaved in the fcc Structure

plane	cross-sectional area of the unit cell (A)[a]	number of connections in two-dimensional unit cell (N)	density of connections (NA^{-1})
{111}	$\sqrt{3}/2$	3	3.5
{100}	1	4	4
{110}	$\sqrt{2}$	6	4.2

[a]Cross-sectional area of the two-dimensional unit cell is normalized by D^2, where D is the diameter of the nanoparticle.

hard-sphere packing of silica nanoparticles, in which packing density is maximized.[28] Therefore, binary colloidal crystals are promising for creation of a wide variety of new three-dimensional mesoscale structures. Several researchers and we have shown that the arrangements of silica nanoparticles can be replicated with carbon,[30a] metal oxides,[36] zeolites,[37] ceramics,[38] metals,[39] and polymers;[40] however, all of them showed the fcc structure. Our binary colloidal crystals can be extended to their templates. Moreover, Yu et al. reported the hard-sphere packing of silicate–micelle composites into the fcc arrangement and their transformation into highly ordered mesoporous silica,[41] to which the present strategy can be extended.

Two-dimensional replication gives a synergistic effect for the diversity of mesoscale surface patterns. The extended three-dimensional mesoscale structures by formation of binary colloidal crystals are further replicated into three- and two-dimensional nanostructures. Techniques of two-dimensional replications to form replicas of other strongly bonded planes of colloidal crystals are challenges to create various nanostructured patterns. This unique concept means that truly new mesoscale structures will be created by the present system. As we mentioned previously,[19] dimpled gold nanoplates can arrange nanoparticles periodically on their dimples. The present products are expected to arrange two kinds of nanoparticles with different sizes in various arrangements. Thus, the variety of dimpled gold nanoplates makes it possible for them to be applied as building blocks of anisotropically and hierarchically structured materials.

■ CONCLUSIONS

We demonstrated that the variety of surface patterns on dimpled gold nanoplates is extended by use of binary colloidal crystals as flexible templates. Such a diversity of mesoscale structures gives us important insights on the mechanisms of two-dimensional replication. Use of a binary colloidal crystal with AlB_2-type structure gives information on the selectivity of surface patterns. The most weakly connected planes are likely to be cleaved during the templating process. Use of a binary colloidal crystal with the $NaZn_{13}$-type structure has indicated that formation of well-defined fractured surfaces on binary colloidal crystals, which should be related to the complexity of mesoscale structures, is crucial to formation of highly ordered dimpled gold nanoplates. The significant points of the present findings are similarity between crystals in classical chemistry and colloidal crystals in mesoscale chemistry and synergism of a crystal-like property of colloidal crystals and templating technique. These ideas lead to extension of surface patterns of dimpled gold nanoplates which are expected to be useful in catalysis, electronics, and optics. We believe that the design of periodic nanospaces in porous materials like colloidal crystals is of growing importance beyond their current applications, such as reactors, supports, adsorbents, etc. These applications utilize not their periodicity but their porosity and uniformity (high surface area and molecular sieving effects). Only periodic

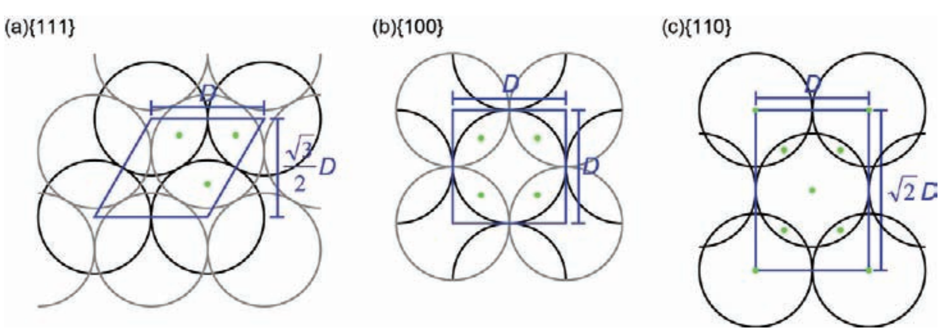

Figure 7. Models of the fcc structure on (a) {111}, (b) {100}, and (c) {110} planes. Black and gray lines indicate the outlines of nanoparticles on upper and lower layers of a cleavage, respectively. Blue lines indicate the two-dimensional unit cell of each plane. Green dots indicate particle–particle connections between the upper and the lower layers.

nanostructures can provide such useful reaction spaces for the syntheses of complex nanostructured materials

■ ASSOCIATED CONTENT

Ⓢ Supporting Information

Transparency of flakes of binary colloidal crystals; calculation of the number of particle−particle connections per unit area for the AlB_2-type structure with smaller **B** nanoparticles. This material is available free of charge via the Internet at http://pubs.acs.org.

■ AUTHOR INFORMATION

Corresponding Author

E-mail: kuroda@waseda.jp

Present Address

‖Department of Applied Chemistry, School of Engineering, The University of Tokyo, 7-3-1 Hongo, Bunkyo-ku, Tokyo 113-8656, Japan.

Notes

The authors declare no competing financial interest.

■ ACKNOWLEDGMENTS

The authors are grateful to Prof. Osamu Terasaki (KAIST and Stockholm University), Ms. Yuriko Kamagata (Waseda University), and Mr. Kazuyuki Ito (Waseda University) for their experimental support. This work was supported by the Elements Science and Technology Project and the Global COE program "Practical Chemical Wisdom" from MEXT, Japan. Y.K. is grateful for financial support via a Grant-in-Aid for JSPS Fellows from MEXT. Y.S. is grateful for financial support by SCF (Special Coordination Funds for Promoting Science and Technology) of MEXT.

■ REFERENCES

(1) Xia, Y.; Xiong, Y. J.; Lim, B.; Skrabalak, S. E. *Angew. Chem., Int. Ed.* **2009**, *48*, 60−103.

(2) (a) Link, S.; El-Sayed, M. A. *J. Phys. Chem. B* **1999**, *103*, 8410−8426. (b) Ghosh, S. K.; Pal, T. *Chem. Rev.* **2007**, *107*, 4797−4862. (c) Jones, M. R.; Osberg, K. D.; Macfarlane, R. J.; Langille, M. R.; Mirkin, C. A. *Chem. Rev.* **2011**, *111*, 3736−3827.

(3) (a) Carmeli, I.; Leitus, G.; Naaman, R.; Reich, S.; Vager, Z. *J. Chem. Phys.* **2003**, *118*, 10372−10375. (b) Jun, Y.-W.; Seo, J.-W.; Cheon, J. *Acc. Chem. Res.* **2008**, *41*, 179−189.

(4) (a) Schlögl, R.; Hamid, S. B. A. *Angew. Chem., Int. Ed.* **2004**, *43*, 1628−1637. (b) Narayanan, R.; El-Sayed, M. A. *J. Phys. Chem. B* **2005**, *109*, 12663−12676.

(5) Perez, J.; Gonzalez, E. R.; Ticianelli, E. A. *Electrochim. Acta* **1998**, *44*, 1329−1339.

(6) (a) Haynes, C. L.; McFarland, A. D.; Van Duyne, R. P. *Anal. Chem.* **2005**, *77*, 338A−346A. (b) Szamocki, R.; Reculusa, S.; Ravaine, S.; Bartlett, P. N.; Kuhn, A.; Hampelmann, R. *Angew. Chem., Int. Ed.* **2006**, *45*, 1317−1321.

(7) (a) Lewis, L. N. *Chem. Rev.* **1993**, *93*, 2693−2730. (b) Haruta, M. *Cattech* **2002**, *6*, 102−115. (c) Zielasek, V.; Jürgens, B.; Schulz, C.; Biener, J.; Biener, M. M.; Hamza, A. V.; Bäumer, M. *Angew. Chem., Int. Ed.* **2006**, *45*, 8241−8244. (d) Wittstock, A.; Zielasek, V; Biener, J.; Friend, C. M.; Bäumer, M. *Science* **2010**, *327*, 319−322. (e) Asao, N.; Ishikawa, Y.; Hatakeyama, N.; Menggenbateer; Yamamoto, Y.; Chen, M.; Zhang, W.; Inoue, A. *Angew. Chem., Int. Ed.* **2010**, *49*, 10093−10095.

(8) Ling, G.; Lu, W.; Cui, W.; Jiang, L. *Cryst. Growth Des.* **2010**, *10*, 1118−1123.

(9) Kim, F.; Connor, S.; Song, H.; Kuykendall, T.; Yang, P. D. *Angew. Chem., Int. Ed.* **2004**, *43*, 3673−3677.

(10) Gao, J. X.; Bender, C. M.; Murphy, C. J. *Langmuir* **2003**, *19*, 9065−9070.

(11) Liu, M. Z.; Guyot-Sionnest, P. *J. Phys. Chem. B* **2005**, *109*, 22192−22200.

(12) Lee, J.-H.; Kamada, K.; Enomoto, N.; Hojo, J. *Cryst. Growth Des.* **2008**, *8*, 2638−2645.

(13) Lofton, C.; Sigmund, W. *Adv. Funct. Mater.* **2005**, *15*, 1197−1208.

(14) Yamauchi, Y; Kuroda, K. *Chem.-Asian J.* **2008**, *3*, 664−676.

(15) Yamauchi, Y.; Tonegawa, A.; Komatsu, M.; Wang, H.; Wang, L.; Nemoto, Y.; Suzuki, N.; Kuroda, K. *J. Am. Chem. Soc.* **2012**, *134*, 5100−5109.

(16) Attard, G. S.; Bartlett, P. N.; Coleman, N. R. B.; Elliott, J. M.; Owen, J. R.; Wang, J. H. *Science* **1997**, *278*, 838−840.

(17) (a) Yamauchi, Y.; Sugiyama, A.; Morimoto, R.; Takai, A.; Kuroda, K. *Angew. Chem., Int. Ed.* **2008**, *47*, 5371−5373. (b) Warren, S. C.; Messina, L. C.; Slaughter, L. S.; Kamperman, M.; Zhou, Q.; Gruner, S. M.; DiSalvo, F. J.; Wiesner, U. *Science* **2008**, *320*, 1748−1752.

(18) Shin, H. J.; Ryoo, R.; Liu, Z.; Terasaki, O. *J. Am. Chem. Soc.* **2001**, *123*, 1246−1247.

(19) Kuroda, Y.; Kuroda, K. *Angew. Chem., Int. Ed.* **2010**, *49*, 6993−6997.

(20) (a) Li, J.; Wang, L.-H.; Liu, L.; Guo, L.; Han, X.-D.; Zhang, Z. *Chem. Commun.* **2010**, *46*, 5109−5111. (b) Zhang, J.; Langille, M. R.; Personick, M. L.; Zhang, K.; Li, S.-Y.; Mirkin, C. A. *J. Am. Chem. Soc.* **2010**, *132*, 14012−14014.

(21) Zhang, J.-M.; Ma, F.; Xu, K.-W. *Appl. Surf. Sci.* **2004**, *229*, 34−42.

(22) Li, Z.; Li, W.; Camargo, P. H. C.; Xia, Y. *Angew. Chem., Int. Ed.* **2008**, *47*, 9653−9656.

(23) Fu, M.; Zhou, J.; Xiao, Q.; Li, B.; Zong, R.; Chen, W.; Zhang, J. *Adv. Mater.* **2006**, *18*, 1001−1004.

(24) Xia, Y.; Lim, B. *Nature* **2010**, *467*, 923−924.

(25) (a) Shevchenko, E. V.; Talapin, D. V.; Kotov, N. A.; O'Brien, S.; Murray, C. B. *Nature* **2006**, *439*, 55−59. (b) Shevchenko, E. V.; Talapin, D. V.; Murray, C. B.; O'Brien, S. *J. Am. Chem. Soc.* **2006**, *128*, 3620−3637. (c) Kalsin, A. M.; Fialkowski, M.; Paszewski, M.; Smoukov, S. K.; Bishop, K. J. M.; Grzybowski, B. A. *Science* **2006**, *312*, 420−424. (d) Evers, W. H.; Friedrich, H.; Filion, L.; Dijkstra, M.; Vanmaekelbergh, D. *Angew. Chem., Int. Ed.* **2009**, *48*, 9655−9657. (e) Chen, J.; Ye, X.; Murray, C. B. *ACS Nano* **2010**, *4*, 2374−2381.

(26) (a) Urban, J. J.; Talapin, D. V.; Shevchenko, E. V.; Kagan, C. R.; Murray, C. B. *Nat. Mater.* **2007**, *6*, 115−121. (b) Dong, A.; Chen, J.; Vora, P. M.; Kikkawa, J. M.; Murray, C. B. *Nature* **2010**, *466*, 474−477.

(27) The definition of mesoscale depends on the science fields, but in this case mesoscale means a size of 10−50 nm.

(28) (a) Sanders, J. V. *Philos. Mag. A* **1980**, *42*, 705−720. (b) Sanders, J. V.; Murray, M. J. *Nature* **1978**, *275*, 201−203.

(29) (a) Wong, S.; Kitaev, V.; Ozin, G. A. *J. Am. Chem. Soc.* **2003**, *125*, 15589−15598. (b) Wang, J.; Ahl, S.; Li, Q.; Kreiter, M.; Neuman, T.; Burkert, K.; Knoll, W.; Jonas, U. *J. Mater. Chem.* **2008**, *18*, 981−988.

(30) (a) Yokoi, T.; Sakamoto, Y.; Terasaki, O.; Kubota, Y.; Okubo, T.; Tatsumi, T. *J. Am. Chem. Soc.* **2006**, *128*, 13664−13665. (b) Davis, T. M.; Snyder, M. A.; Krohn, J. E.; Tsapatsis, M. *Chem. Mater.* **2006**, *18*, 5814−5816. (c) Snyder, M. A.; Lee, J. A.; Davis, M. T.; Scriven, L. E.; Tsapatsis, M. *Langmuir* **2007**, *23*, 9924−9928. (d) Yokoi, T.; Wakabayashi, J.; Otsuka, Y.; Fan, W.; Iwama, M.; Watanabe, R.; Aramaki, K.; Shimojima, A.; Tatsumi, T.; Okubo, T. *Chem. Mater.* **2009**, *21*, 3719−3729.

(31) Hartlen, K. D.; Athanasopoulos, A. P. T.; Kitaev, V. *Langmuir* **2008**, *24*, 1714−1720.

(32) Unary colloidal crystals consisting of silica nanoparticles could be formed from all of the dispersions used in this study, which suggested that the grown silica nanoparticles were monodispersed and the nucleation of silica nanoparticles did not occur during the growth

process. Detailed conditions to suppress nucleation have precisely been investigated in ref 31.
(33) (a) Murray, M. J.; Sanders, J. V. *Philos. Mag. A* **1980**, *42*, 721−740. (b) Eldridge, M. D.; Madden, P. A.; Frenkel, D. *Nature* **1993**, *365*, 35−37. (c) Cottin, X.; Monson, P. A. *J. Chem. Phys.* **1995**, *102*, 3354−3360. (d) Filion, L.; Marechal, M.; van Oorschot, B.; Pelt, D.; Smallenburg, F.; Dijkstra, M. *Phys. Rev. Lett.* **2009**, *103*, 188302.
(34) The lattice constants of binary colloidal crystals possess some deviations, and averaged values in several TEM images are indicated.
(35) (a) Gao, C. B.; Sakamoto, Y.; Terasaki, O.; Che, S.-N. *Chem.—Eur. J.* **2008**, *14*, 11423−11428. (b) Sakamoto, Y.; Han, L.; Che, S.-N.; Terasaki, O. *Chem. Mater.* **2009**, *21*, 223−229. (c) Han, L.; Sakamoto, Y.; Che, S.-N.; Terasaki, O. *Chem.—Eur. J.* **2009**, *15*, 2818−2825.
(36) Yokoi, T.; Sakuma, J.; Maeda, K.; Domen, K.; Tatsumi, T.; Kondo, J. N. *Phys. Chem. Chem. Phys.* **2011**, *13*, 2563−2570.
(37) Fan, W.; Snyder, M. A.; Kumar, S.; Lee, P.-S.; Yoo, W. C.; McCormick, A. V.; Penn, R. L.; Stein, A.; Tsapatsis, M. *Nat. Mater.* **2008**, *7*, 984−991.
(38) Fukasawa, Y.; Takanabe, K.; Shimojima, A.; Antonietti, M.; Domen, K.; Okubo, T. *Chem.—Asian J.* **2011**, *6*, 103−109.
(39) (a) Egan, G. L.; Yu, J. S.; Kim, C. H.; Lee, S. J.; Schaak, R. E.; Mallouk, T. E. *Adv. Mater.* **2000**, *12*, 1040−1042. (b) Kuroda, Y.; Yamauchi, Y.; Kuroda, K. *Chem. Commun.* **2010**, *46*, 1827−1829.
(40) Johnson, S. A.; Ollivier, P. J.; Mallouk, T. E. *Science* **1999**, *283*, 963−965.
(41) (a) Tang, J.-W.; Zhou, X.-F.; Zhao, D.-Y.; Lu, G. Q.; Zou, J.; Yu, C.-Z. *J. Am. Chem. Soc.* **2007**, *129*, 9044−9048. (b) Yuan, P.; Sun, J.-L.; Xu, H.-Y.; Zhou, L.; Liu, J.-Z.; Zhang, D.-L.; Wang, Y.-H.; Jack, K. S.; Drennan, J.; Zhao, D.-Y.; Lu, G.-Q.; Zou, X.-D.; Zou, J.; Yu, C.-Z. *Chem. Mater.* **2011**, *23*, 229−238.